International Journal of Advanced Nuclear Reactor Design and Technology 3 (2021) 74–79

Contents lists available at ScienceDirect

International Journal of Advanced Nuclear Reactor Design and Technology

journal homepage: www.sciencedirect.com/journal/international-journal-of-advanced-nuclear-reactor-design-and-technology

Effect of LaB_6 addition on mechanical properties and irradiation resistance of 316L stainless steels processed by selective laser melting

Dexin Xu [a], Feida Chen [a,c,*], Xiaobin Tang [a,b], Lida Shen [d], Jiabin Jiang [d], Zhangjie Sun [a], Songyuan Li [a], Zhenlong Geng [a]

[a] Department of Nuclear Science and Technology, Nanjing University of Aeronautics and Astronautics, Nanjing, 211106, China
[b] Key Laboratory of Nuclear Technology Application and Radiation Protection in Astronautics, Nanjing University of Aeronautics and Astronautics, Ministry of Industry and Information Technology, Nanjing, 211106, China
[c] Jiangsu Engineering Laboratory of Nuclear Energy Equipment Materials, Nanjing, 211106, China
[d] College of Mechanical and Electrical Engineering, Nanjing University of Aeronautics and Astronautics, Yu Dao Street, Nanjing, 210016, China

ARTICLE INFO

Keywords:
Selective laser melting
LaB_6 reinforced 316L SS
Ion irradiation
Mechanical properties
Irradiation resistance

ABSTRACT

The 316L stainless steels (SS) have become one of the most common structural materials in nuclear system applications due to their excellent physicochemical performance. Selective laser melting (SLM) preparation, mechanical properties, and irradiation resistance of 316L SS reinforced by second-phase particles have aroused extensive attention. Here, the mechanical properties of 316L SS with different LaB_6 contents processed by SLM before irradiation and the irradiation-induced swelling after 50 keV He^+ irradiation at room temperature were investigated. Results showed that the microstructure was refined with the LaB_6 addition, and the size of 316L SS subgrains decreased with the increase of LaB_6. LaB_6 reinforced 316L SS (316L-LaB_6) exhibited higher hardness and yield strength compared with 316L SS without LaB_6 addition. After 50 keV He^+ irradiation, the irradiation-induced swelling rate of 316L-LaB_6 was lower than that of 316L SS without LaB_6 addition, indicating that LaB_6 improved the irradiation resistance of 316L SS. Consequently, our study indicated the potential of using 316L-LaB_6 as irradiation-resistant material.

1. Introduction

The current research commonly focuses on the strength and irradiation resistance of second-phase reinforced metal materials in the field of nuclear materials [1,2]. Based on the latest second-phase enhancement theory, the nano second phase refines the matrix structure and greatly improves the strength of materials by pinning dislocations to hinder their movement [3–7]. Second-phase particles have significant effects on improving the strength and toughness of metal materials [8,9]. AlMangour et al. [10] prepared nanocomposites with high compressive yield strength and ductility at room and high temperatures by adding TiB_2 to 316L stainless steel. In addition, the nano-sized second-phase particles can greatly promote the annihilation rate of irradiation-induced defects in materials, which results in the improvement of their irradiation resistance [11–14]. Therefore, strengthening metal materials by adding second-phase particles is a feasible method.

316L stainless steels (SS) are one of the most common structural materials in nuclear system applications due to their excellent performance and low price [15]. However, the structure of nuclear energy equipment, such as spent fuel storage racks, is sophisticated and presents difficulties in the formation with traditional manufacturing processes. Additive manufacturing (AM) technology possesses advantages in reducing production steps and improving the flexibility for complex geometric structures [16]. Selective laser melting (SLM) [17] is an emerging AM laser technology characterized by design freedom and one-step forming, which can reduce the cost and time consumption of nuclear structural material. Thus, it has great application prospects and potential in manufacturing nuclear energy equipment [18]. On the other hand, a strong neutron radioactivity exists in the spent fuel storage environment. Therefore, the strength and irradiation resistance of spent fuel storage materials must be improved to ensure the reliability of spent fuel storage materials in long-term services. The preparation and mechanical properties of AM metal materials reinforced by second-phase particles have aroused widespread attention [19–21]; however, the studies on their irradiation resistance are limited.

LaB_6 has a high melting point, good chemical stability, strong

* Corresponding author. Department of Nuclear Science and Technology, Nanjing University of Aeronautics and Astronautics, Nanjing, 211106, China.
E-mail address: fdchen@nuaa.edu.cn (F. Chen).

https://doi.org/10.1016/j.jandt.2021.06.004
Received 10 April 2021; Received in revised form 17 June 2021; Accepted 17 June 2021
Available online 3 July 2021

irradiation resistance and other excellent properties [22,23]. This compound is expected to improve the strength and irradiation resistance of 316L SS, specifically by adding the second-phase LaB_6 particles into 316L SS [24–28]. Therefore, this paper adopted SLM process to prepare 316L SS materials added with LaB_6 particles. The changes in mechanical properties of 316L SS under different forming processes were explored, and the effects of LaB_6 content on the microstructure, mechanical properties, and irradiation resistance of 316L SS were evaluated with the microscopic, mechanical and irradiation swelling studies.

2. Materials and experiments

The diameters of 316L SS powders used in this work were between 30 and 50 μm, and the average size of LaB_6 powders was 50 nm. The two kinds of powders were mixed and ball milled in argon atmosphere. The milling speed and time were 200 rpm and 500 min, respectively, with a 1:1.5 ball material ratio. Fig. 1(a) and (b) show the micro morphology of 316L/LaB_6 mixed powders after ball milling.

The samples were manufactured using a selective laser melting (SLM) machine (NCL-M2120 equipped with maximum power of 200 W). A total of 140 and 180 W power were selected for printing samples. Each layer (n) was rotated 67° with respect to the previous layer (n-1) as depicted in Fig. 1(c). All the samples were processed by SLM. After optimizing LaB_6 content, the 316L SS with three LaB_6 contents (0%, 0.01%, and 0.1%, weight fraction) were selected for subsequent experiments. In the following, L0, L0.01, and L0.1 are used to represent 316L SS samples with 0%, 0.01%, and 0.1% LaB_6 addition, respectively. Fig. 1 (d) shows the bulk samples processed by SLM.

Irradiation experiments were performed on the 320 kV platform at the Institute of Modern Physics, Chinese Academy of Sciences (CAS). The samples were irradiated with 50 keV He^+ to 30 dpa at room temperature. According to the calculation results of SRIM program [29], the damage peak was at the depth of 160 nm and He^+ concentration peak was 0.8 at.% at the depth of 200 nm. Characterizing the irradiation-induced swelling of the materials is one of the methods to study their irradiation resistance. Therefore, half of the surface of each sample was covered by aluminum foil during the irradiation to characterize the degree of swelling.

The phase structures of polished samples were identified by X-ray diffraction (XRD, Rigaku Ultima IV with Cu K-alpha radiation) operated at 40 kV voltage and 40 mA current. Vickers hardness and small punch test (SPT) were used to characterize the mechanical properties of the samples. SPT was carried out on a Shimadzu universal mechanical experiment machine with a maximum load of 5 kN, and the size of the wafer sample was $\phi 10 \times 0.5\ mm^3$. The microstructures of samples were characterized by SEM (TESCAN LYRA3 GM at a working voltage of 20 kV) and transmission electron microscopy (TEM, FEI Talos F200X operated at 200 kV), and the distribution of elements was analyzed by energy dispersive X-ray spectroscopy (EDS). Atomic force microscopy (AFM, Bruker Dimension Icon) was adopted to measure the relative height of boundary between irradiated and unirradiated regions. The average relative height was measured from five different positions on the boundary between irradiated and unirradiated regions for each sample to avoid accidents.

3. Results

3.1. Microstructures

Fig. 2(a) shows the XRD results of samples before irradiation. All the samples showed FCC austenite diffraction peaks of γ(111), γ(200), and γ(220). Different SLM processes showed no evident influence on the phase structures but changed the intensity of the diffraction peak and full width half maximum (FWHM). In all the samples added with LaB_6, the characteristic peaks of LaB_6 were inconspicuous because minor phases were undetectable at volumes ≤5 wt%, given the limitation of

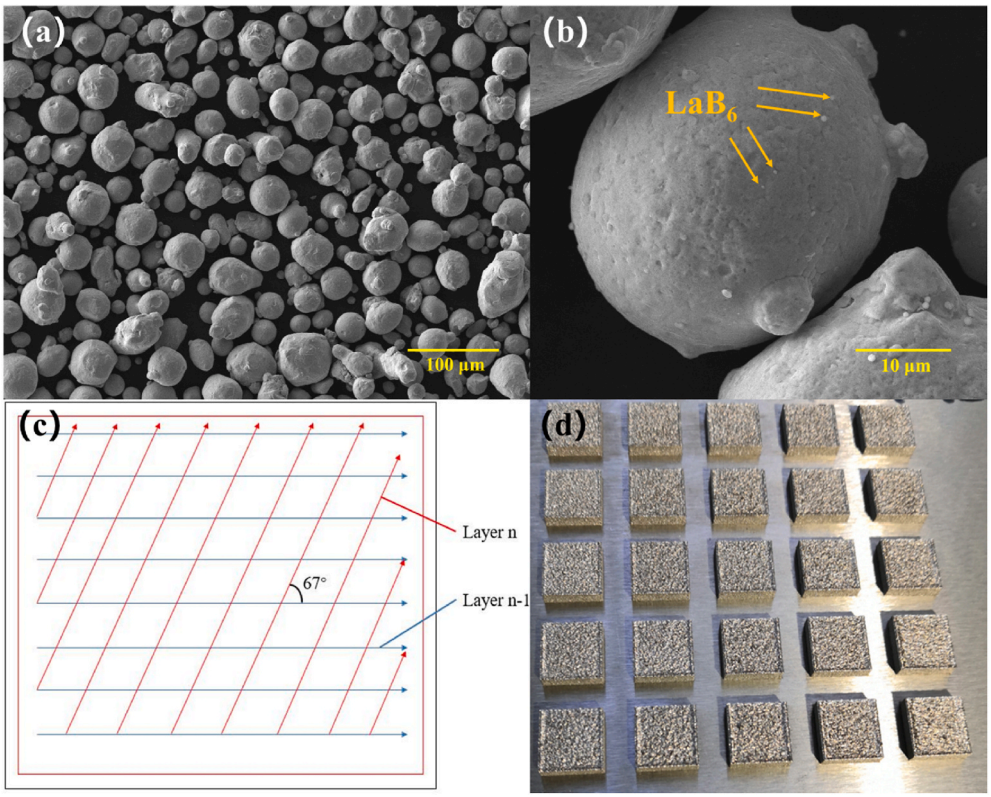

Fig. 1. (a) and (b) Scanning electron microscopy (SEM) images of 316L/LaB_6 mixed powder after ball milling. (c) SLM scanning strategy. (d) Bulk sample processed by SLM.

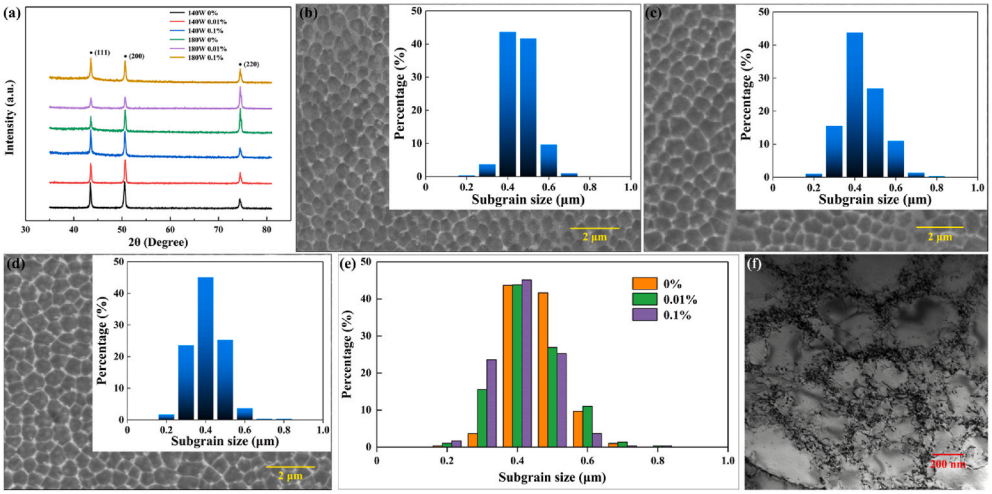

Fig. 2. (a) XRD results of 140 and 180 W samples. SEM images and corresponding subgrain size distribution of (b) L0, (c) L0.01, and (d) L0.1 sample. (e) Statistical distribution results of subgrain size of L0, L0.01, and L0.1 sample. (f) TEM image of 316L SS subgrains.

the detection instrument.

Fig. 2(b)–(d) show the SEM microstructures of L0, L0.01, and L0.1 samples at 180 W, respectively. The cellular subgrain structure, which is a unique structural feature of SLM-processed materials, can be observed clearly in all the samples. The subgrain sizes and distribution of L0, L0.01, and L0.1 samples were counted, and the statistical results are shown in Fig. 2(e). The subgrain sizes of all the samples were mainly concentrated in the 400–500 nm range. With the increase of LaB_6 content, the proportion of subgrains with sizes of 500–600 nm decreased, whereas the proportion of subgrains measuring around 300 nm increased. The average subgrain sizes of L0, L0.01, and L0.1 samples were calculated as 0.41, 0.38 and 0.35 μm, respectively. This finding indicates that the addition of LaB_6 reduced the subgrain size, which proves that the addition of second-phase particles has the positive effect of grain refinement.

The microstructure was characterized by TEM to further understand the microstructure of the material. The subgrains can be observed distinctly in the TEM image shown in Fig. 2(f). The calculated size of subgrains was about 400 nm, which corresponds to the SEM results. In addition, numerous particles were homogenously distributed in the material (Fig. 3(a)). EDS showed that the particles were silicon oxide, whose formation was caused by the reaction between the trace silicon in the powder and oxygen in the SLM process. Specifically, oxygen was probably derived from natural oxides on the surface of the powder and oxygen impurities in the SLM process atmosphere. Although conducted in a vacuum treatment prior to printing, there may still be residual oxygen. Due to the strong affinity between O element and Si, the Si element in the powder naturally combines with O to form an oxide during the laser melting process. A similar phenomenon was observed in the report of Sun et al. [30] and Lin et al. [31].

3.2. Hardness and SPT

Fig. 4 shows the Vickers hardness of samples with the increase of LaB_6 content under different powers. In the case of 140 W, the hardness of samples increased as the amount of LaB_6 increased. When 0.01% LaB_6 was added, the hardness of L0.01 sample significantly improved from 231 HV to 238 HV. While the content of LaB_6 increased to 0.1%, the increase of hardness was not evident. According to Hall-Petch model [32], the grain refinement is an important strengthening mechanism. In previous studies, Ertugrul et al. [33] found that the addition of the second-phase TiC particles refined the grain size of 316L based coating. At the same time, TiC addition increased the hardness of the 316L based coating by about 100 HV. Therefore, the average subgrain size of 316L SS gradually decreased as LaB_6 increased, which improved the hardness of the material. In the case of 180 W, the hardness of L0.01 sample was higher than that of L0 sample. However, when LaB_6 content increased to 0.1%, the hardness of L0.1 sample decreased from 259 HV to 243 HV compared with that of L0.01 sample. On the premise that the process has been optimized, the slight increase in the number of hole defects during solidification of the sample may be responsible for the decrease in hardness. This finding indicates that the content of LaB_6 cannot be

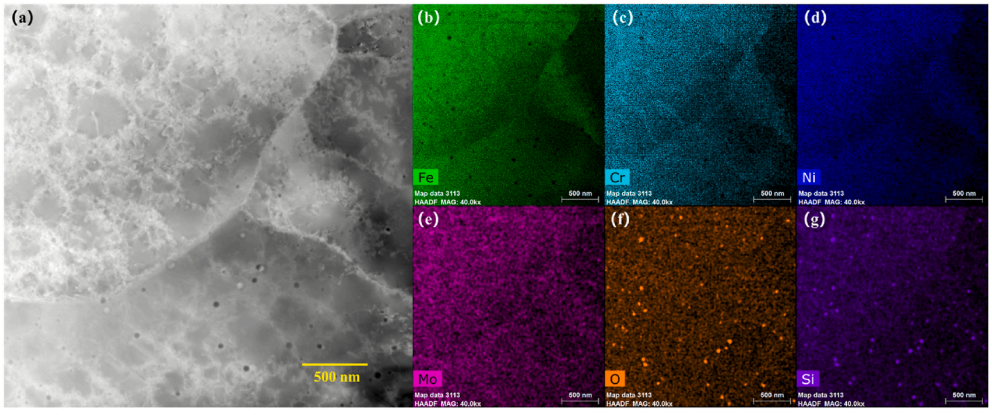

Fig. 3. (a) TEM image of 316L sample. Corresponding EDS mapping of (b) Fe, (c) Cr, (d) Ni, (e) Mo, (f) O, and (g) Si.

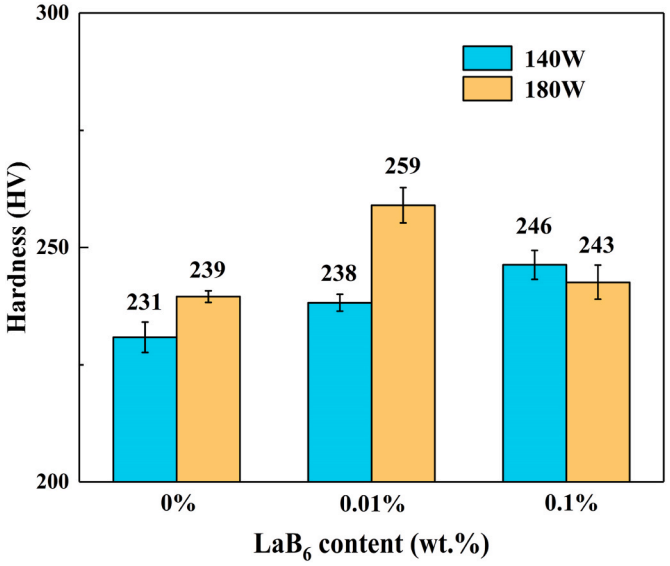

Fig. 4. Vickers hardness of 140 and 180 W samples with different LaB_6 contents.

increased constantly under this process. Although the hardness of L0.1 sample decreased, it was higher than that of L0 sample under the same condition. In addition, a laser with a power of 180 W melt the powders more completely compared with 140 W, resulting in a material with lower porosity and higher hardness.

As the hardness of the samples manufactured at 180 W is higher than that of the samples at 140 W, indicating that the quality of 180 W samples was better than that of the 140 W samples, subsequent studies were only conducted on the samples manufactured at 180 W. Fig. 5(a) and (b) show the fracture surface morphology of the small punch samples. The fracture surface was crescent shaped. A large number of dimples can be observed on the fracture surface in Fig. 5(b), indicating that it is a ductile fracture. Fig. 5(c) shows the load-displacement curve of L0, L0.01, and L0.1 samples at 180 W, from which the mechanical properties of the samples can be evaluated. Table 1 shows the yield load, ultimate load and fracture energy of samples calculated from Fig. 5(c). The yield load reflects the yield strength of the material. Table 1 shows that with the increase of LaB_6, the yield strength of the sample increased, indicating that the addition of LaB_6 enhanced the yield strength of the material. The ultimate load and fracture energy reflect the ultimate

Table 1
Yield strength, ultimate load and fracture energy of 316L SS with different LaB_6 contents calculated from Fig. 5(c).

LaB_6 content (wt.%)	Yield load (N)	Ultimate load (N)	Fracture energy (mJ)
0%	276.87	1410.62	1326.52
0.01%	390.94	1659.69	1668.82
0.1%	470.47	1229.22	1533.96

tensile strength and ductility of the material respectively. After adding 0.01% LaB_6, the ultimate tensile strength and ductility of the samples improved, proving the strengthening effect of LaB_6. According to the SEM results, LaB_6 affects refining of subgrains by increasing the number of interfaces in the material. Given the pinning effect of subgrain boundaries and nano precipitated phase on dislocation movement, the yield strength of the material was improved [24,28,34]. Previous studies have also shown that the addition of the second-phase particles refined the grain size and increased the yield strength of 316L SS [10,35]. However, when LaB_6 content increased to 0.1%, the ultimate tensile strength and ductility of L0.1 sample decreased, which may be caused by the slight decrease in material density due to hole defects during solidification of the sample. Overall, the addition of LaB_6 improved the mechanical properties of the studied materials.

3.3. *Irradiation-induced swelling*

AFM test was performed at the boundary between irradiated and unirradiated regions to characterize the degree of irradiation swelling of the samples. The results are shown in Fig. 6. According to the statistics results, the step heights of L0, L0.01, and L0.1 samples were measured to be 49.872, 41.303 and 27.145 nm, respectively. The corresponding swelling rates were calculated as 13.12% (L0), 10.87% (L0.01) and 7.14% (L0.1). The irradiation swelling rates of L0.01 and L0.1 samples decreased compared with that of the L0 sample, indicating that LaB_6 inhibited the irradiation swelling of 316L SS. LaB_6 may inhibit the nucleation and growth of helium bubbles, thereby reducing the swelling of the material. Specifically, LaB_6 promotes the annihilation and reorganization of point defects, resulting in the decreased number of effective defects. On the other hand, LaB_6 captures He atoms and vacancies and inhibits their accumulation and growth. Note that the peak at the boundary of the irradiated and unirradiated regions may be caused by the accumulation of target atoms alongside aluminum foil as the sample swelled during the irradiation [36]. In addition, as the content of LaB_6 increased, the swelling rate of the sample decreased, which indicates

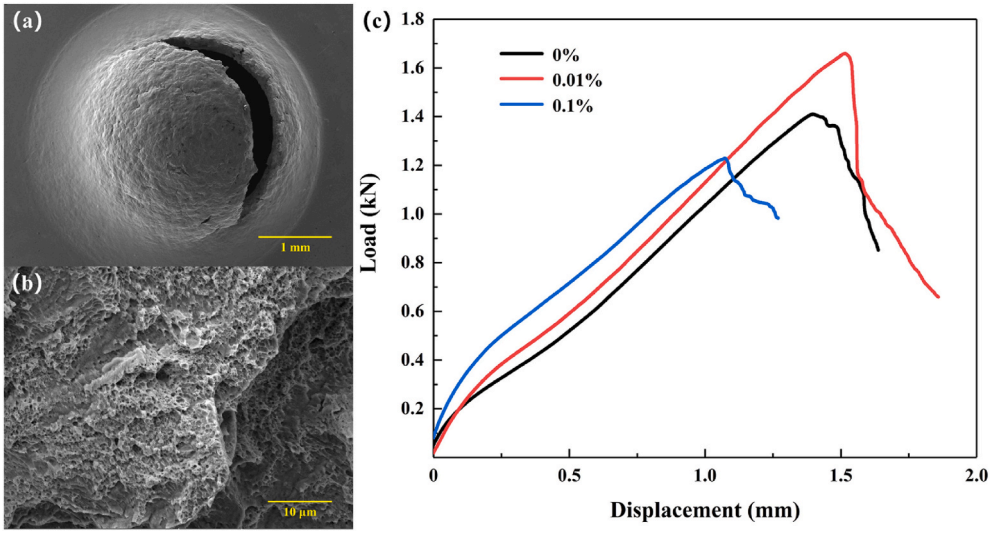

Fig. 5. (a) and (b) Fracture surface morphology of the small punch samples. (c) Load-displacement curve of 316L SS with different LaB_6 contents.

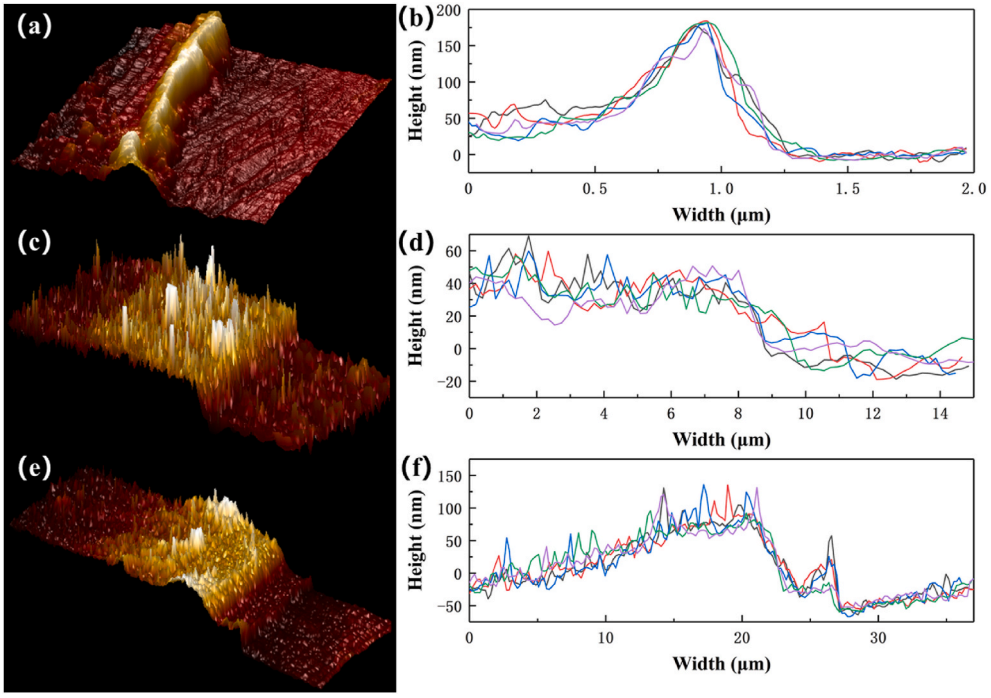

Fig. 6. AFM images near the boundary between irradiated and unirradiated regions of (a) L0, (c) L0.01 and (e) L0.1 sample. (b), (d), and (f) Corresponding surface relative heights.

that LaB_6 improved the irradiation resistance of the material to a certain extent.

4. Conclusion

LaB_6 reinforced 316L SS (316L-LaB_6) processed by SLM was irradiated by 50 keV He^+ to 30 dpa at room temperature. A series of experimental studies was conducted on the mechanical properties and irradiation swelling of 316L SS with different LaB_6 contents. On this basis, we observed that 316L-LaB_6 exhibited improved mechanical properties and irradiation resistance compared with 316L SS without LaB_6 addition. The main conclusions of this study are as follows:

1. 316L SS processed by SLM has a special cellular substructure. With the increase of LaB_6 content, the size of subgrains decreased, which indicates that LaB_6 possesses the effect of grain refinement.
2. The hardness, yield strength, and tensile strength of the samples improved after the addition of LaB_6. Thus, LaB_6 enhanced the mechanical properties of 316L SS. This result is due to the subgrain refinement and increased interface density of 316L SS caused by LaB_6. Thereby the movement of dislocations was further hindered, which led to the improvement of the mechanical properties of 316L SS.
3. The irradiation swelling rate of 316L SS decreased from 13.12% to 7.14% as the content of LaB_6 increased from 0% to 0.1% after 50 keV He^+ irradiation. LaB_6 reduced the swelling rate of 316L SS by inhibiting the nucleation and growth of helium bubbles. The results showed that LaB_6 improved the irradiation resistance of 316L SS.

Declaration of competing interest

The authors declare that they have no known competing financial interests or personal relationships that could have appeared to influence the work reported in this paper.

Acknowledgments

This work is supported from the National Natural Science Foundation of China (Grant No. 11705087), and the project supported by China Postdoctoral Science Foundation (Grant No. 2020M671488).

References

[1] M.E. Mahmoud, A.M. El-Khatib, R.M. El-Sharkawy, A.R. Rashad, M.S. Badawi, M. A. Gepreel, Design and testing of high-density polyethylene nanocomposites filled with lead oxide micro- and nano-particles: mechanical, thermal, and morphological properties, J. Appl. Polym. Sci. (2019), https://doi.org/10.1002/app.47812.
[2] Z. Lei, X. Liu, Y. Wu, H. Wang, S. Jiang, S. Wang, X. Hui, Y. Wu, B. Gault, P. Kontis, D. Raabe, L. Gu, Q. Zhang, H. Chen, H. Wang, J. Liu, K. An, Q. Zeng, T.G. Nieh, Z. Lu, Enhanced strength and ductility in a high-entropy alloy via ordered oxygen complexes, Nature (2018), https://doi.org/10.1038/s41586-018-0685-y.
[3] J.H. Martin, B.D. Yahata, J.M. Hundley, J.A. Mayer, T.A. Schaedler, T.M. Pollock, 3D printing of high-strength aluminium alloys, Nature (2017), https://doi.org/10.1038/nature23894.
[4] M.J. Bermingham, S.D. McDonald, M.S. Dargusch, Effect of trace lanthanum hexaboride and boron additions on microstructure, tensile properties and anisotropy of Ti-6Al-4V produced by additive manufacturing, Mater. Sci. Eng., A (2018), https://doi.org/10.1016/j.msea.2018.02.012.
[5] T. Borkar, S. Nag, Y. Ren, J. Tiley, R. Banerjee, Reactive spark plasma sintering (SPS) of nitride reinforced titanium alloy composites, J. Alloys Compd. (2014), https://doi.org/10.1016/j.jallcom.2014.08.049.
[6] D. Handtrack, F. Despang, C. Sauer, B. Kieback, N. Reinfried, Y. Grin, Fabrication of ultra-fine grained and dispersion-strengthened titanium materials by spark plasma sintering, Mater. Sci. Eng., A (2006), https://doi.org/10.1016/j.msea.2006.07.143.
[7] M.J. Bermingham, D. Kent, H. Zhan, D.H. Stjohn, M.S. Dargusch, Controlling the microstructure and properties of wire arc additive manufactured Ti-6Al-4V with trace boron additions, Acta Mater. (2015), https://doi.org/10.1016/j.actamat.2015.03.035.
[8] B. AlMangour, D. Grzesiak, Jenn-MingYang, Selective laser melting of TiC reinforced 316L stainless steel matrix nanocomposites: influence of starting TiC particle size and volume content, Mater. Des. (2016), https://doi.org/10.1016/j.matdes.2016.05.018.
[9] I. Sulima, M. Perek-Nowak, L. Jaworska, P. Wyżga, The influence of reinforcing particles on mechanical and tribological properties and microstructure of the steel-TiB 2 composites, J. Achiev. Mater. Manuf. Eng. (2011).
[10] B. AlMangour, Y.K. Kim, D. Grzesiak, K.A. Lee, Novel TiB2-reinforced 316L stainless steel nanocomposites with excellent room- and high-temperature yield strength developed by additive manufacturing, Compos. B Eng. (2019), https://doi.org/10.1016/j.compositesb.2018.07.050.

[11] S. Shen, F. Chen, X. Tang, J. Lin, G. Ge, J. Liu, Effects of carbon doping on irradiation resistance of Fe38Mn40Ni11Al4Cr7 high entropy alloys, J. Nucl. Mater. (2020), https://doi.org/10.1016/j.jnucmat.2020.152380.
[12] S. Shen, F. Chen, X. Tang, G. Ge, J. Gao, Z. Sun, Irradiation damage and swelling of carbon-doped Fe38Mn40Ni11Al4Cr7 high-entropy alloys under heavy ion irradiation at elevated temperature, J. Mater. Sci. (2020), https://doi.org/10.1007/s10853-020-05229-7.
[13] R. Lindau, A. Möslang, M. Schirra, P. Schlossmacher, M. Klimenkov, Mechanical and microstructural properties of a hipped RAFM ODS-steel, J. Nucl. Mater. (2002), https://doi.org/10.1016/S0022-3115(02)01045-0.
[14] P. Song, D. Morrall, Z. Zhang, K. Yabuuchi, A. Kimura, Radiation response of ODS ferritic steels with different oxide particles under ion-irradiation at 550 °C, J. Nucl. Mater. (2018), https://doi.org/10.1016/j.jnucmat.2018.02.007.
[15] S. Wang, J. Li, Y. Cao, B. Gao, Q. Mao, Y. Li, Thermal stability and tensile property of 316L stainless steel with heterogeneous lamella structure, Vacuum (2018), https://doi.org/10.1016/j.vacuum.2018.03.040.
[16] J.J. Lewandowski, M. Seifi, Metal additive manufacturing: a review of mechanical properties, Annu. Rev. Mater. Res. (2016), https://doi.org/10.1146/annurev-matsci-070115-032024.
[17] X.P. Li, G. Ji, Z. Chen, A. Addad, Y. Wu, H.W. Wang, J. Vleugels, J. Van Humbeeck, J.P. Kruth, Selective laser melting of nano-TiB2decorated AlSi10Mg alloy with high fracture strength and ductility, Acta Mater. (2017), https://doi.org/10.1016/j.actamat.2017.02.062.
[18] Y. Zhong, L.E. Rännar, S. Wikman, A. Koptyug, L. Liu, D. Cui, Z. Shen, Additive manufacturing of ITER first wall panel parts by two approaches: selective laser melting and electron beam melting, Fusion Eng. Des. (2017), https://doi.org/10.1016/j.fusengdes.2017.01.032.
[19] F. Akhtar, P. Feng, X. Du, A.S. Jawid, J. Tian, S. Guo, Microstructure and property evolution during the sintering of stainless steel alloy with Si3N4, Mater. Sci. Eng., A (2008), https://doi.org/10.1016/j.msea.2007.04.032.
[20] J. Dutta Majumdar, A. Kumar, L. Li, Direct laser cladding of SiC dispersed AISI 316L stainless steel, Tribol. Int. (2009), https://doi.org/10.1016/j.triboint.2008.10.016.
[21] B. AlMangour, D. Grzesiak, T. Borkar, J.M. Yang, Densification behavior, microstructural evolution, and mechanical properties of TiC/316L stainless steel nanocomposites fabricated by selective laser melting, Mater. Des. (2018), https://doi.org/10.1016/j.matdes.2017.10.039.
[22] M. Aono, R. Nishitani, C. Oshima, T. Tanaka, E. Bannai, S. Kawai, LaB6 and SmB6 (001) surfaces studied by angle-resolved XPS, LEED and ISS, Surf. Sci. (1979), https://doi.org/10.1016/0039-6028(79)90443-6.
[23] Y. Furukawa, M. Yamabe, A. Itoh, T. Inagaki, Emission characteristics of single-crystal LaB 6 cathodes with ⟨100⟩ and ⟨110⟩ orientations, J. Vac. Sci. Technol. (1982), https://doi.org/10.1116/1.571357.
[24] Y. Feng, K. Feng, C. Yao, Z. Li, Effect of LaB6 addition on the microstructure and properties of (Ti3Al + TiB)/Ti composites by laser cladding, Mater. Des. (2019), https://doi.org/10.1016/j.matdes.2019.107959.
[25] Z. Qiankun, J. Yao, S. Weijun, Z. Huibin, H. Yuehui, L. Nan, C.T. Liu, H. Han, H. Xiaolin, Direct fabrication of high-performance high speed steel products enhanced by LaB6, Mater. Des. (2016), https://doi.org/10.1016/j.matdes.2016.09.044.
[26] S.K. Kashyap, R. Mitra, Effect of LaB 6 additions on densification, microstructure, and creep with oxide scale formation in ZrB 2 -SiC composites sintered by spark plasma sintering, J. Eur. Ceram. Soc. (2019), https://doi.org/10.1016/j.jeurceramsoc.2019.03.043.
[27] W. Shen, B. Nan, W. Wang, L. Yu, Q. Zhang, Y. He, X. Huang, G. Yuan, In situ synthesis and strengthening of ultra high-carbon martensitic stainless steels in addition of LaB6, J. Alloys Compd. (2018), https://doi.org/10.1016/j.jallcom.2017.12.195.
[28] M. Liu, S. Liu, W. Chen, C. Chen, Y. Lv, X. Zhang, P. Lei, Y. Lin, K. Zhou, Effect of trace lanthanum hexaboride on the phase, grain structure, and texture of electron beam melted Ti-6Al-4V, Addit. Manuf. (2019), https://doi.org/10.1016/j.addma.2019.100873.
[29] J.F. Ziegler, M.D. Ziegler, J.P. Biersack, SRIM - the stopping and range of ions in matter, Nucl. Instrum. Methods Phys. Res. Sect. B Beam Interact. Mater. Atoms (2010), https://doi.org/10.1016/j.nimb.2010.02.091, 2010.
[30] X. Sun, F. Chen, H. Huang, J. Lin, X. Tang, Effects of interfaces on the helium bubble formation and radiation hardening of an austenitic stainless steel achieved by additive manufacturing, Appl. Surf. Sci. (2019), https://doi.org/10.1016/j.apsusc.2018.10.268.
[31] J. Lin, F. Chen, X. Tang, J. Liu, S. Shen, G. Ge, Radiation-induced swelling and hardening of 316L stainless steel fabricated by selected laser melting, Vacuum (2020), https://doi.org/10.1016/j.vacuum.2020.109183.
[32] A. Loucif, R.B. Figueiredo, T. Baudin, F. Brisset, R. Chemam, T.G. Langdon, Ultrafine grains and the Hall-Petch relationship in an Al-Mg-Si alloy processed by high-pressure torsion, Mater. Sci. Eng., A 532 (2012) 139–145, https://doi.org/10.1016/j.msea.2011.10.074.
[33] O. Ertugrul, T.M. Enrici, H. Paydas, E. Saggionetto, F. Boschini, A. Mertens, Laser cladding of TiC reinforced 316L stainless steel composites: feedstock powder preparation and microstructural evaluation, Powder Technol. (2020), https://doi.org/10.1016/j.powtec.2020.07.100.
[34] Y. Zhao, J. Sun, J. Li, Effect of rare earth oxide on the properties of laser cladding layer and machining vibration suppressing in side milling, Appl. Surf. Sci. (2014), https://doi.org/10.1016/j.apsusc.2014.09.195.
[35] O.O. Salman, C. Gammer, J. Eckert, M.Z. Salih, E.H. Abdulsalam, K.G. Prashanth, S. Scudino, Selective laser melting of 316L stainless steel: influence of TiB2 addition on microstructure and mechanical properties, Mater. Today Commun. (2019), https://doi.org/10.1016/j.mtcomm.2019.100615.
[36] S. Chang, K.K. Tseng, T.Y. Yang, D.S. Chao, J.W. Yeh, J.H. Liang, Irradiation-induced swelling and hardening in HfNbTaTiZr refractory high-entropy alloy, Mater. Lett. 272 (2020), https://doi.org/10.1016/j.matlet.2020.127832.